Amidrazone Analogues of D-Ribofuranose as Transition-State Inhibitors of Nucleoside Hydrolase[†]

Markus Boutellier,[‡] Benjamin A. Horenstein,[§,∥] Alexi Semenyaka,[§] Vern L. Schramm,[*,§] and Bruce Ganem[*,‡]

Department of Chemistry, Baker Laboratory, Cornell University, Ithaca, New York 14853-1301, and Department of Biochemistry, Albert Einstein College of Medicine, 1300 Morris Park Avenue, Bronx, New York 10461

ABSTRACT: The transition state of inosine during hydrolysis by nucleoside hydrolase has been characterized by kinetic isotope effects, bond-energy/bond-order vibrational analysis, and molecular electrostatic potential surface calculations [Horenstein, B. A., Parkin, D. W., Estupinan, B., & Schramm, V. L. (1991) *Biochemistry* **30**, 10788–10795; Horenstein, B. A., & Schramm, V. L. (1993) *Biochemistry* **32**, 7089–7097]. The heterocyclic base is protonated and the anomeric carbon of the ribofuranosyl ring is flattened to form a transition-state with extensive oxocarbenium ion character. With their delocalized charge and flattened structures, amidrazone analogues of D-ribofuranose provide both geometric and electronic mimics of the ribosyl group at the transition-state of nucleoside hydrolase. A family of riboamidrazones was synthesized with H, phenyl, and *p*-nitrophenyl N-substituents. The analogues were competitive inhibitors with respect to inosine and gave K_i values of 10^{-5}, 2×10^{-7}, and 1×10^{-8} M, respectively. (*p*-Nitrophenyl)riboamidrazone exhibited slow-onset, tight-binding inhibition, with an overall dissociation constant of 2×10^{-9} M. The binding is reversible with an off-rate of 3×10^{-3} s^{-1}. Tight binding can be attributed to the close spatial match between the molecular geometry of (*p*-nitrophenyl)riboamidrazone and the transition-state stabilized by nucleoside hydrolase. The favorable binding interactions of the (*p*-nitrophenyl)riboamidrazone include oxocarbenium ion mimicry, isosteric ribosyl hydroxyls, and hydrophobic and H-bonding interactions at the nitrophenyl group. Analysis of the conformational space available to the (*p*-nitrophenyl)riboamidrazone indicates that the geometry that approximates the enzyme-stabilized transition state is 7–14 kcal/mol unfavorable relative to the global conformational minimum for free inhibitor. The apparent overall K_d of 2 nM represents only a fraction of the intrinsic energy available for transition-state interactions with nucleoside hydrolase. When corrected for the energy of distortion required to achieve the transition-state conformation, (*p*-nitrophenyl)riboamidrazone binds with an affinity near that expected for an ideal transition-state analogue.

The cleavage of C–N glycosidic bonds is promoted by a family of enzymes that includes the NAD+ hydrolases, nucleoside and nucleotide nucleosidases, and nucleoside phosphorylases. These enzymes are involved in pathways of purine and pyrimidine pool regulation and salvage (Leung & Schramm, 1980; Parkin et al., 1991), base-excision repair mechanisms of DNA (Sancar & Sancar, 1988), and inactivation of ribosomes (Endo et al., 1991), as well as hydrolysis of NAD+ and polymerization of ADP ribose from NAD+ [e.g., Tarnus et al. (1988)]. Several enzymes from this family have been characterized by kinetic isotope effects and by transition-state analysis [e.g., Mentch et al. (1987) and Horenstein et al. (1991)].

The transition states for the C–N glycohydrolases characterized to date exhibit protonation of the aglycone leaving groups, oxocarbenium ion character in the ribosyl group, well-developed C–N bond dissociation, weak preassociation of a water or anionic nucleophile, and a flattened, sp²-like anomeric carbon center in the ribose ring. A prototype for these enzymes

is the nucleoside hydrolase of *Crithidia fasciculata* (Parkin et al., 1991). This organism is a trypanosome parasite of the mosquito and provides an example of the parasitic protozoa that are incapable of de novo purine synthesis and require purine salvage enzymes for survival. Nucleoside hydrolase (eq 1) converts purine and pyrimidine ribonucleosides to ribose and the constituent bases. A comparison of the geometric structure for inosine and for inosine at the transition state of nucleoside hydrolase is shown in Figure 1A,B.

$$\text{nucleoside} + \text{H}_2\text{O} \rightarrow \text{base} + \text{ribose} \qquad (1)$$
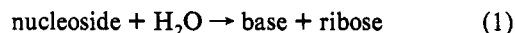
With their delocalized charge and flattened structures, the amide derivatives **1–4** (Table 1) electronically and geometrically resemble the transition state for nucleoside hydrolase. These compounds were considered to have potential as nucleoside hydrolase inhibitors by analogy to the six-membered amidines, amidrazones, and amidoximes, which are good competitive inhibitors of exoglycosidases (Ganem & Papandreou, 1991; Papandreou et al., 1993). Comparison of **4** with the transition-state for nucleoside hydrolase by molecular model building demonstrates similar geometry and charge features for the transition state (compare Figure 1B with C and D). The freedom of rotation around the amidrazone N–N and C–N single bonds (labeled α and β, Figure 2) was expected to permit the aglycon to reach an optimal conformation for both the hydrophobic and hydrogen-bonding features of the transition state. Recent success in applying transition-state analysis to the design of inhibitory

---

[*] Address correspondence to these authors.
[‡] Cornell University.
[§] Albert Einstein College of Medicine.
[∥] Current address: Department of Chemistry, University of Florida, Gainesville, FL 32611.
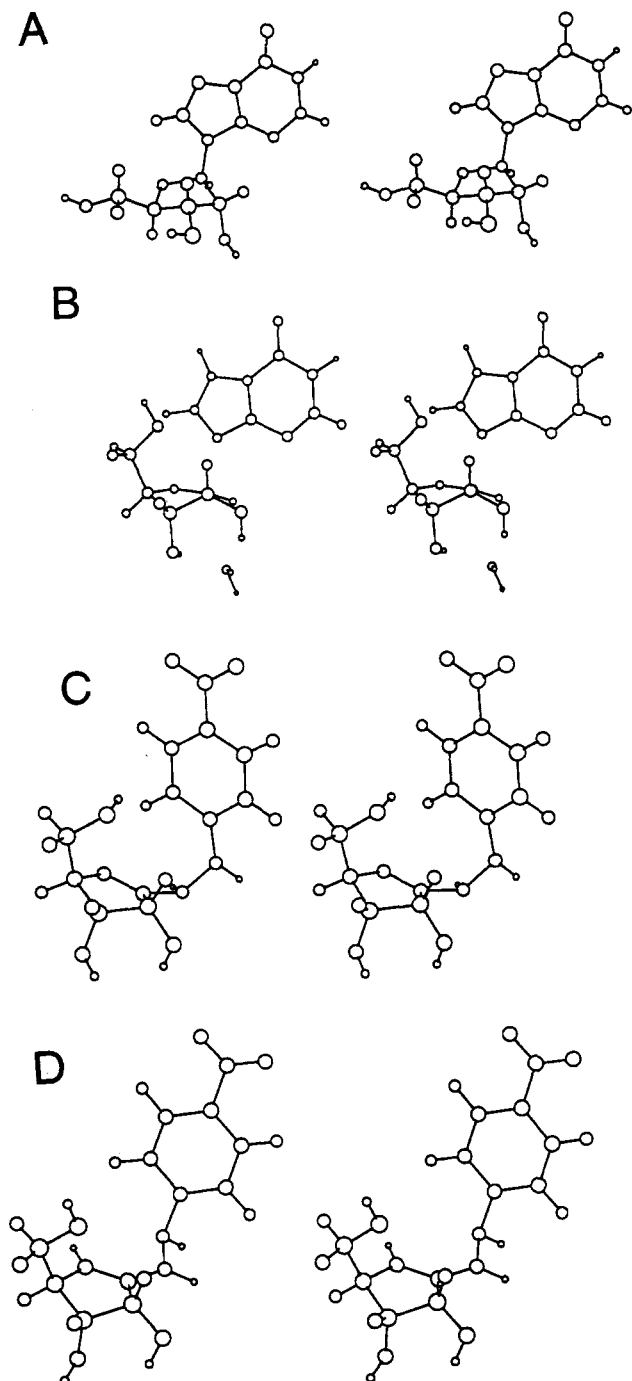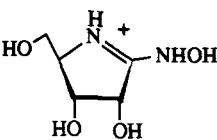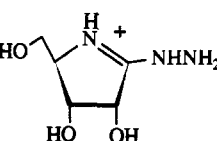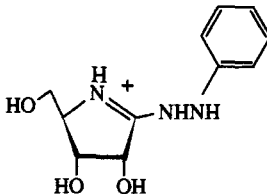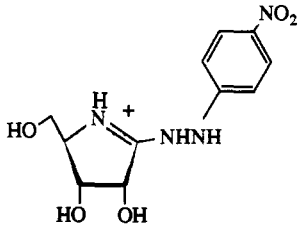
FIGURE 1: Stereoview images of inosine (A), the transition-state structure for inosine stabilized by nucleoside hydrolase (B), and both N_4'-unprotonated (C) and N_4'-protonated (D) (p-nitrophenyl)-riboamidrazone 4 presented in conformations near that for the transition-state (compare B–D). The structure of inosine is from X-ray crystal data (Munns & Tollin, 1970), and the transition-state (B) was established by kinetic isotope effect studies (Horenstein et al., 1991). The transition state features protonation of N7 in the imidazole portion of the purine, extensive bond loss to ribose, 3'-exo configuration of the ribose ring, and weak participation of the water nucleophile, shown 3 Å below the ribosyl ring. The (p-nitrophenyl)-riboamidrazone in both C and D is oriented in conformations near that of the transition-state.

C-glycosides of 1,4-dideoxy-4-aminoribitol (Horenstein & Schramm, 1993a,b) indicated the importance of the inclusion of aglycon mimicry in effective transition-state analogues.

The results with (p-nitrophenyl)riboamidrazone 4 indicate that slow-onset inhibition occurs when both geometric, charge, and hydrogen-bonding features of the transition-state are

Table 1: Amidoxime and Amidrazone Inhibitors of Nucleoside Hydrolase

inhibitor	K_i	K_m/K_i
riboamidoxime (**1**)	>50 μM[a]	≥ 1
riboamidrazone (**2**)	10 μM[b]	38
phenylriboamidrazone (**3**)	0.21 ± 0.01[c] μM	1810
p-nitrophenylriboamidrazone (**4**)	10 ± 4[c] nM	3.8 x 10⁴
	2 ± 1[d] nM	1.9 x 10⁵

[a] No inhibition was observed at 10 μM using inosine at a concentration of 300 μM. [b] Assayed at a single inosine concentration of 380 μM. [c] Determined by best-fit analysis to the equation for competitive inhibition during initial rate conditions. [d] Equilibrium inhibition constant that includes the slow-onset component (K_i^* of eq 6).

included in the inhibitor. Molecular mechanics analysis of the amidrazones established that (p-nitrophenyl)riboamidrazone **4** includes key features of the transition state. The equilibrium binding constant of 2 nM for **4** makes this nucleoside analogue the most powerful inhibitor currently developed for nucleoside hydrolase.

EXPERIMENTAL PROCEDURES

General. Solvents were dried and distilled using standard procedures. All reagents were distilled or recrystallized prior to use. Anhydrous hydroxylamine was prepared by adding hydroxylamine sulfate to anhydrous liquid ammonia, whereupon ammonium sulfate precipitated. After the evaporation of ammonia, the residue was triturated with anhydrous CH_3-OH and the solution filtered through Celite. NMR spectra were measured on a Bruker AF 300 spectrometer, with chemical shifts reported in ppm and the residual solvent signal as reference. IR spectra were recorded on a Mattson Galaxy FT-IR. Mass spectra (MS) were measured on a VG 70-VSE (EI) or a VG ZAB-SE (FAB) instrument. The synthesis of 1–4 in Table 1 is summarized in Scheme 1.

(3R,4R,5R)-3,4-Dihydroxy-5-(hydroxymethyl)-2-pyrro-lidinone (7). Dry ammonia (10 mL, distilled from sodium metal) was condensed under argon into a 100-mL, three-neck, round-bottom flask containing the N,O-dibenzylated

Scheme 1
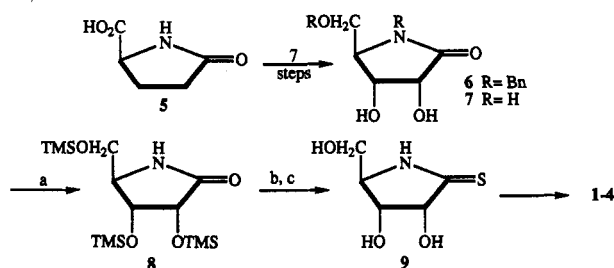
a Reagents: (a) 10 equiv of (TMS)₂NH, 10 equiv of TMSCl, and pyr; (b) 1.1 equiv of Lawesson's reagent and C₆H₆, reflux for 1 h; (c) HCl/ MeOH, room temperature, 20 min, 70% from **7**.

lactam **6** (160 mg, 0.49 mmol) and equipped with a dry ice/ acetone condenser and stir bar. Small pieces of sodium (0.5–1 mmol) were added in portions until a dark blue color persisted. After the mixture was stirred for 3.5 h, ethanol (2–3 drops) was added and the reaction was warmed to room temperature. The ammonia was evaporated and the residue was loaded onto a Dowex 50X8 column (H⁺-form, 200–400 mesh). Ion-exchange chromatography eluted with H_2O (3-mL fractions) afforded lactam **7** (40 mg, 0.27 mmol): ¹H NMR (300 MHz, D₂O) δ 3.40–3.45 (m, 1H), 3.48–3.55 (m, 2H), 4.12 (d, *J* = 5.5 Hz, 1H), 4.29 (d, *J* = 5.5 Hz, 1H); ¹³C NMR (75 MHz, D₂O) δ 62.4, 62.6, 71.0, 71.1, 178.4; EI-MS *m/z* 148 (M + 1), 129, 116, 98, 88, 72; IR (KBr) 1675, 1280, 1130, 1050 cm⁻¹.

(3R,4R,5R)-N-(Trimethylsilyl)-3,4-bis[(trimethylsilyl)-oxy]-5-[[(trimethylsilyl)oxy]methyl]-2-pyrrolidinone (**8**). Lactam **7** (30 mg, 0.20 mmol) was suspended under argon in anhydrous pyridine (2 mL) in a 5-mL round-bottom flask. The suspension was cooled to 0 °C, and hexamethyldisilazane (430 μL, 2.04 mmol) was added dropwise, followed by chlorotrimethylsilane (260 μL, 2.04 mmol). After 15 min at 0 °C, the reaction was warmed to room temperature and stirred for 2 h. Pyridine was evaporated, and the residue was triturated with hexanes (40 × 1 mL) and filtered through Celite. Evaporation of the solvent afforded persilylated lactam **8** (86 mg, 0.19 mmol), which was used without further purification: ¹H NMR (300 MHz, CDCl₃) δ 0.097 (s, 3H), 0.105 (s, 3H), 0.17 (s, 3H), 0.26 (s, 3H), 3.30–3.42 (m, 2H), 3.56 (dd, *J* = 3.5, 10 Hz, 1H), 4.18 (d, *J* = 5 Hz, 1H), 4.37 (d, *J* = 5 Hz, 1H); EI-MS *m/z* 435 (M⁺), 420, 348, 332, 217, 170, 147; IR (KBr) 2950, 1680, 1250, 1170, 1100 cm⁻¹.

(3R,4R,5R)-3,4-Dihydroxy-5-(hydroxymethyl)-2-thion-opyrrolidinone (**9**). A mixture of silylated lactam **8** (28 mg, 64 μmol), freshly recrystallized Lawesson's reagent (28 mg, 70 μmol), and anhydrous benzene (2 mL) under argon was slowly heated to reflux. After 1 h, the reaction mixture was cooled to room temperature and concentrated *in vacuo*. The residue was redissolved in anhydrous CH₃OH (2 mL), acidified with methanolic 4 N HCl (2 drops), and stirred for 0.5 h to desilylate the product. The resulting solution was concentrated, and the residue was triturated first with CHCl₃ and then with CH₃OH. The combined CH₃OH extracts (25 × 1 mL) were filtered through Celite and evaporated. The crude material was purified by column chromatography on SiO₂ (CH₂Cl₂/CH₃OH/NH₄OH, 7:3:1), giving thionolactam **9** (8 mg, 49 mol): ¹H NMR (300 MHz, D₂O) δ 3.50–3.63 (m, 3H), 4.15 (dd, *J* = 5.5, 1 Hz, 1H), 4.32 (d, *J* = 5.5 Hz, 1H); ¹³C NMR (75 MHz, D₂O) δ 61.7, 69.4, 72.2, 79.3, 205.9; EI-MS *m/z* 163 (M⁺), 132, 114, 104, 87; IR (KBr) 1540, 1290, 1150 cm⁻¹.

D-*Riboamidoxime* (**1**). To a solution of thionolactam **9** (4.8 mg, 30 μmol) in dry CH₃OH (1 mL) was added excess anhydrous hydroxylamine (20 mg, 0.67 mmol) in CH₃OH (450 μL) at 0 °C under argon. After stirring at room temperature for 18 h, the reaction mixture was concentrated *in vacuo* to a viscous oil, which was redissolved in water (2 mL) and lyophilized to afford amidoxime **1** (4.5 mg, 93%), which was pure by TLC and NMR: ¹H NMR (300 MHz, D₂O) δ 3.50–3.53 (m, 2H), 3.56–3.58 (m, 1H), 4.07 (dd, *J* = 5.5, 2.5 Hz, 1H), 4.63 (d, *J* = 5.5 Hz, 1H); ¹³C NMR (75 MHz, D₂O) δ 61.9, 66.7, 71.6, 72.1, 163.4; FAB-MS *m/z* 163 (M + 1), 145, 131, 115.

D-*Riboamidrazone* (**2**). To a solution of thionolactam **9** (12 mg, 74 μmol) in dry CH₃OH (1.5 mL) was added anhydrous hydrazine (45 μL, 1.44 mmol) at 0 °C under argon. After stirring at 0 °C for 1 h, the reaction mixture was filtered through Celite and concentrated *in vacuo*. Riboamidrazone **2** (12 mg, quantitative yield) obtained was pure by TLC and NMR: ¹H NMR (300 MHz, D₂O) δ 3.40–3.53 (m, 3H), 4.00 (dd, *J* = 5, 3 Hz, 1H), 4.40 (d, *J* = 5 Hz, 1H); ¹³C NMR (75 MHz, D₂O) δ 62.4, 64.7, 71.5, 71.7, 160.9; FAB-MS *m/z* 162 (M + 1); IR (KBr) 1550, 1400, 1140, 1030 cm⁻¹.

N-*Phenyl*-D-*riboamidrazone* (**3**). To a solution of thiono-lactam **9** (4.2 mg, 26 μmol) in dry CH₃OH (0.5 mL) at 0 °C was added anhydrous phenylhydrazine (25 μL, 0.26 mmol) under argon. After 15 min, the reaction was warmed to 45–50 °C and stirred for 30 h. Concentration *in vacuo*, followed by column chromatography on SiO₂ (CH₂Cl₂, then CH₂Cl₂/ CH₃OH/NH₄OH, 7:3:1), gave D-phenylriboamidrazone **3** (4 mg, 65%): ¹H NMR (300 MHz, D₂O) δ 3.48–3.56 (m, 3H), 4.07–4.10 (m, 1H), 4.61 (d, *J* = 5.5 Hz, 1H), 6.77–6.82 (m, 3H), 7.12–7.17 (m, 2H).

N-*(p-Nitrophenyl)*-D-*riboamidrazone* (**4**). A mixture of thionolactam **9** (8.2 mg, 50 μmol), anhydrous *p*-nitrophen-ylhydrazine (80 mg, 0.52 mmol), and dry CH₃OH (1.5 mL) was warmed to reflux for 6 days. After concentration *in vacuo*, column chromatography on SiO₂ (CH₂Cl₂/CH₃OH, 95:5, then CH₂Cl₂/CH₃OH/NH₄OH, 7:3:1) afforded N-*(p*-ni-trophenyl)-D-riboamidrazone **4** (4 mg, 14 μmol) and unreacted thionolactam **9** (3.2 mg, 20 μmol). The yield of **4**, when corrected for recovered **9**, was 47%: ¹H NMR (300 MHz, D₂O) δ 3.54–3.57 (m, 2H) 3.68–3.71 (m, 1H), 4.22 (dd, *J* = 5.5, 1.5 Hz, 1H), 4.95 (d, *J* = 5.5 Hz, 1H), 6.76–6.80 (m, 2H), 7.95–8.02 (m, 2H).

Assay of Nucleoside Hydrolase. Conversion of inosine to hypoxanthine and ribose was monitored continuously by the change in ultraviolet absorbance, with Δ_{280} = –920 M⁻¹ cm⁻¹. Reactions were initiated by the addition of 1 μL of a nucleoside hydrolase solution to assay mixtures (30 °C) containing 50 mM MES/Bis-Tris mixed buffers (pH 7), the desired inosine concentration, and the indicated concentration of inhibitors.

Determination of K_i Values. Competitive inhibition patterns were established for some inhibitors by full kinetic analysis using a matrix of five substrate and three inhibitor concentrations. The data were analyzed according to the equation for competitive inhibition (Cleland, 1977). In some cases, the inhibitor dissociation constant was estimated by measuring initial reaction rates in the presence of a fixed substrate concentration near the K_m value and varying the inhibitor concentration. This approach was used for slow-onset inhibition, where initial rates were obtained only during the first 2 min of the reaction. In these cases, competitive inhibition was assumed and the K_i was determined from the expression

$$\nu_o/\nu_i = (K_m + A)/(K_m(1 + (I/K_i)) + A) \qquad (2)$$

where ν_o and ν_i are the uninhibited and inhibited initial rates,

I and *A* are inhibitor and substrate concentrations, and K_m and K_i are the Michaelis and inhibitor dissociation constants, respectively.

Analysis of Slow-Onset Inhibition. Slow-onset inhibition was analyzed according to eq 3,

$$E + I \overset{K_i}{\rightleftharpoons} EI \underset{k_6}{\overset{k_5}{\rightleftharpoons}} E^*I \qquad (3)$$
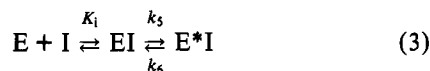
where EI is formed by readily reversible competitive inhibition, described by the dissociation constant K_i, and the slow onset of inhibition is described by the first-order rate constant, k_5, to form the tightly bound complex E*I. The tight-binding component of E*I reverts to EI with rate constant k_6 (Merkler et al., 1990; Morrison & Walsh, 1988).

The first-order rate constant *k* describing the approach to equilibrium for EI and E*I was estimated by fitting the progress of reaction curves to eq 4, where *P* is the amount of product at time *t*, and v_o and v_s represent the initial and final steady-state rates, respectively (Morrison & Stone, 1985). The rate of conversion of E*I to EI (k_6) was estimated by

$$P = v_s t + (v_o - v_s)(1 - e^{-kt})/k \qquad (4)$$

preincubating 400 nM nucleoside hydrolase with 500 nM inhibitor in 50 mM MES/Bis-Tris (pH 7.0) on ice for 70 min. A 1-μL aliquot was added to 1.0 mL of 500 μM inosine in assay buffer. The return of activity was followed as a function of time. The 1:1000 dilution of the incubation mixture into the assay mixture resulted in a final inhibitor concentration of 0.5 nM. A control experiment in which an identical concentration of nucleoside hydrolase was incubated in the absence of inhibitor displayed the same initial reaction rate (within experimental error) as the final reaction rate for the inhibitor-release experiment, indicating sufficient dilution of the E*I complex. The progress of the reaction curve was fit to eq 4 with $v_o = 0$. Using k_6 and *k* determined above, the rate constant, k_5, for the formation of E*I from EI was calculated from

$$k = k_6 + k_5((I/K_i)/(1 + A/K_m + I/I_i)) \qquad (5)$$

The overall inhibition constant for *I* (K_i^*) was calculated from eq 6, where K_i is the dissociation constant for EI.

$$K_i^* = K_i(k_6/(k_5 + k_6)) \qquad (6)$$

Conformational Analysis of p-(Nitrophenyl)amidrazone. Conformational energies for the geometric conformers of **4** were estimated by MOPAC calculations using the AM1 Hamiltonian. The rigid rotor approximation was used after the conformations of both the riboamide and the *p*-nitrophenyl rings were fixed near that of the transition state (e.g., Figure 1B,C). The ribosyl ring was placed in the 3'-exo conformation and frozen during all subsequent calculations since AM1 calculations result in unrealistic flattening of the ring. Calculations were then made at increments around the dihedrals indicated as α and β in Figure 2. Local minima were identified by a search with variable α and β dihedrals to generate a matrix of conformers whose energies were evaluated using the rigid rotor approximation. The initial conformational minima identified by this method were optimized by allowing all coordinates except the ribosyl ring configuration to vary during the minimization. One *local* minimum energy conformation was identified for both unprotonated and protonated **4** with configurations resembling
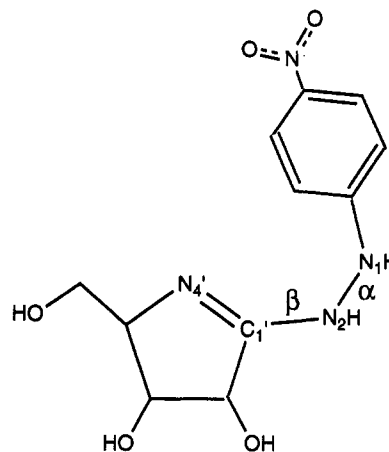

FIGURE 2: Structure of N_4'-unprotonated (*p*-nitrophenyl)riboamidrazone showing the α and β bonds. In this structure, $\alpha = \beta = 0°$ when the atoms *C*-phenyl, N_1, N_2, C_1', and N_4' lie in the same plane, in the configuration shown.

the proposed transition-state structure for nucleoside hydrolase (Horenstein & Schramm, 1993a). In addition, global conformational minima were located for both protonated and unprotonated inhibitors.

RESULTS

Synthesis of Riboamidrazones. The synthesis of **1–4** (Table 1) commenced from the known lactam **6**, which was readily available from (*S*)-pyroglutamic acid **5** (Ikota & Hanaki, 1990). N,O-Debenzylation of **6** by anhydrous dissolving-metal reduction afforded lactam **7**. After silylation, protected lactam **8** was treated with Lawesson's reagent as previously reported (Tong et al., 1990; Ganem & Papandreou, 1991) to furnish thionolactam **9**. Reaction of **9** with excess anhydrous hydroxylamine/methanol at room temperature produced riboamidoxime **1** in 93% yield. Titration of **1** indicated a pK_a of 5.4. Reaction of **9** with anhydrous hydrazine afforded the parent D-ribofuranosylamidrazone **2** in quantitative yield. Titrimetric analysis established a pK_a value of 8.2 for this substance. In similar fashion, reaction of **9** with excess anhydrous phenylhydrazine (CH_3OH, 45–50 °C, 30 h) or *p*-nitrophenylhydrazine (CH_3OH, reflux, 6 days) produced **3** and **4** in 65% and 47% yields, respectively. Titration of **4** indicated a pK_a value of 5.8. Thionolactam **9** provided a convenient precursor for linking a variety of aglycon to the flattened five-membered heterocyclic ring, which stereochemically and electronically resembled the transition-state of nucleoside hydrolase. This synthetic route has obvious utility in the production of other transition-state inhibitors possessing oxocarbenium ion character.

Initial Rate Inhibition Studies. Nucleoside hydrolase was not significantly inhibited by 10 μM riboamidoxime **1** (Table 1) with substrate fixed at 300 μM, which is slightly below the K_m of 380 μM. Thus, the inhibition constant for **1** was greater than 50 μM. Riboamidrazone **2** (Table 1) exhibited significant inhibition when tested at micromolar concentrations in the presence of 300 μM inosine and gave an apparent dissociation constant of 10 μM when analyzed according to eq 2. Phenylriboamidrazone **3** was a slope-linear competitive inhibitor with a K_i of 207 ± 13 nM when subjected to full kinetic analysis (Table 1). Preincubation of enzyme and inhibitor did not alter initial rates, and no slow-onset component could be detected when initial rate measurements were extended to 20 min. Thus, phenylriboamidrazone **3** was a classic competitive inhibitor. Initial rate analysis with (*p*-

FIGURE 4: Reaction mechanism for nucleoside hydrolase, including the slow-onset inhibition by (*p*-nitrophenyl)riboamidrazone **4**. The upper line is the uninhibited reaction, K_i is the rapidly reversible binding component of inhibition, and k_5 and k_6 represent the rate constants for formation and relaxation of the tightly bound complex (E*p-nitrophenylamidrazone).

Table 2: Conformational Energies for (*p*-Nitrophenyl)-riboamidrazone at Global and Local Minima and at Transition-State Configurations

inhibitor conformation[a]	dihedral angles[b] (deg)		energy[c] (kcal/mol)
	α	β	
unprotonated 1, global minimum	299	338	−65.1
unprotonated 2, local minimum	61	19	−63.6
unprotonated 3, local minimum	258	199	−61.1
protonated 1, global minimum	124	7	78.2
protonated 2, local minimum	311	3	80.2
protonated 3, local minimum	276	186	80.3
ts geometry 1, unprotonated	326	97	−51.5
ts geometry 2, unprotonated	80	5	−49.1
ts geometry 1, protonated	102	5	85.6
ts geometry 2, protonated	326	97	102.9

[a] Each group of inhibitor conformations includes conformations with the most closely related structural energy minima, calculated as described in the Experimental Procedures. [b] Dihedral angles are defined in Figure 2. [c] Conformational energies for the same species are comparable. Energies for species differing in protonation state are not comparable.
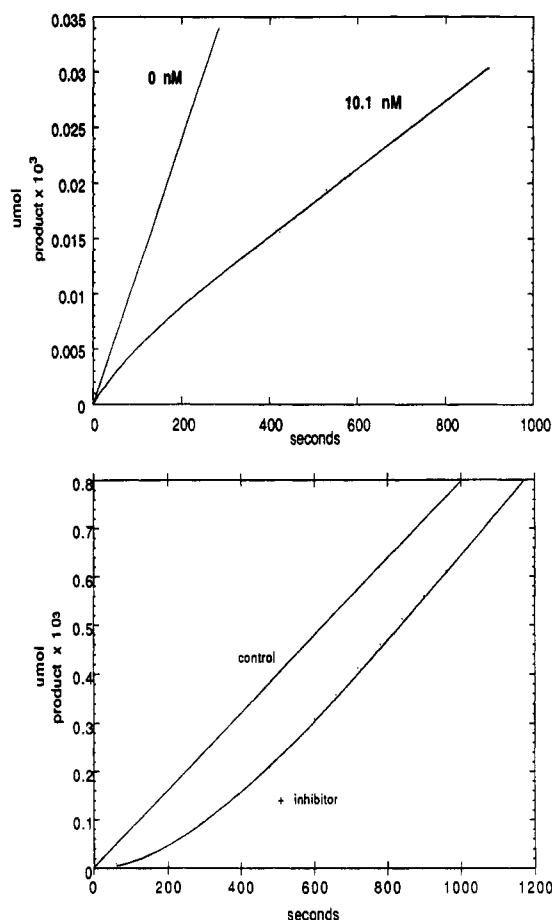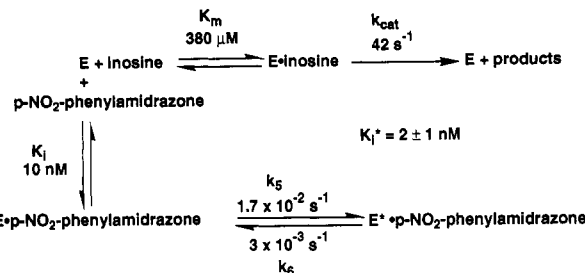

FIGURE 3: Slow-onset inhibition (upper panel) and slow inhibitor release (lower panel) for (*p*-nitrophenyl)riboamidrazone **4** with nucleoside hydrolase. Rates of product formation were measured at 500 μM inosine using the continuous recording assay. The data were digitized by hand and fit to the equations described in the text. The lines represent the best fits to the equations. The upper panel compares a control (0 nM) reaction rate with an identical assay containing 10.1 nM inhibitor. The lower panel demonstrates activity regained following the dilution of fully inhibited enzyme into assay mixture. The control experiment was the same as the "+ inhibitor" curve, except that no inhibitor was included in the incubation. Conditions for the experiment are provided in the Experimental Procedures.

nitrophenyl)riboamidrazone **4** gave a competitive inhibition pattern and a K_i of 10 ± 3.6 nM. The initial rates were short-lived and were followed by the slow onset of a second inhibitory component.

Analysis of Slow-Onset Inhibition and Activity Regain. Addition of nucleoside hydrolase to reaction mixtures containing inosine and (*p*-nitrophenyl)riboamidrazone **4** gave inhibited initial rates of short duration, followed by a second phase of inhibition which reached a new steady state after several additional minutes (Figure 3, upper panel). Experiments at several inhibitor concentrations were analyzed according to eq 4 to give an apparent rate of onset of $k = (7 \pm 2) \times 10^{-3}$ s^{-1}. The rate of E*I conversion to EI (k_6 of eq 3) was determined by the regain of activity when the equilibrium mixture of enzyme and **4** was subjected to a large dilution in excess inosine. Under these conditions, the rate of activity regain approximated k_6. An example of activity regain is shown in Figure 3 (lower panel), together with a *control* of uninhibited enzyme. The first-order regain of activity gave a value for $k_6 = (3.0 \pm 0.2) \times 10^{-3}$ s^{-1}. Equation 5 was solved for $k_5 = (1.7 \pm 0.9) \times 10^{-2}$ s^{-1} using the kinetic and rate constants given above, together with the inhibition curves at two inhibitor concentrations. The equilibrium

dissociation constant for the inhibitor $K_i^* = 2 \pm 1$ nM (eq 6). The kinetic constants for substrate and (*p*-nitrophenyl)-riboamidrazone are summarized in Figure 4.

Conformational Analysis of (p-Nitrophenyl)riboamidrazone (**4**). A search of conformational space within the rigid rotor approximation followed by additional energy refinement of all minima (see Experimental Procedures) located three related minima for both the protonated and unprotonated (*p*-nitrophenyl)amidrazone (**4**). The minima for the protonated compound were within 2 kcal of each other, while those for unprotonated **4** were within 4.5 kcal of each other (Table 2). None of the energetic minima place the nitrophenyl group in a position similar to that of the departing hypoxanthine in the transition state for nucleoside hydrolase, but they are characterized by near-planar angles for the amidrazone (dihedrals near 0° or 180°). Structures corresponding to the energy minima for unprotonated and protonated (*p*-nitrophenyl)amidrazone (shown in Figure 5A,B) are characterized by the nitrophenyl group extending away from the ribosyl group. Movement of the nitrophenyl to a position similar to that for hypoxanthine in the transition-state (Figure 5C,D) can be accomplished for both unprotonated and protonated inhibitors. The energy barrier from the global minimum of the unprotonated inhibitor to the unprotonated transition-state conformation is 13.6 kcal/mol, while the barrier is near 7.4 kcal/mol for the protonated inhibitor (Table 2). The transition-state conformation for protonated **4** is only 7.4 kcal from the global minimum, with $\alpha = 102°$ and $\beta = 5°$. However, superposition of the ribosyl ring of this structure with that of the transition state indicates a 2.5-Å displacement
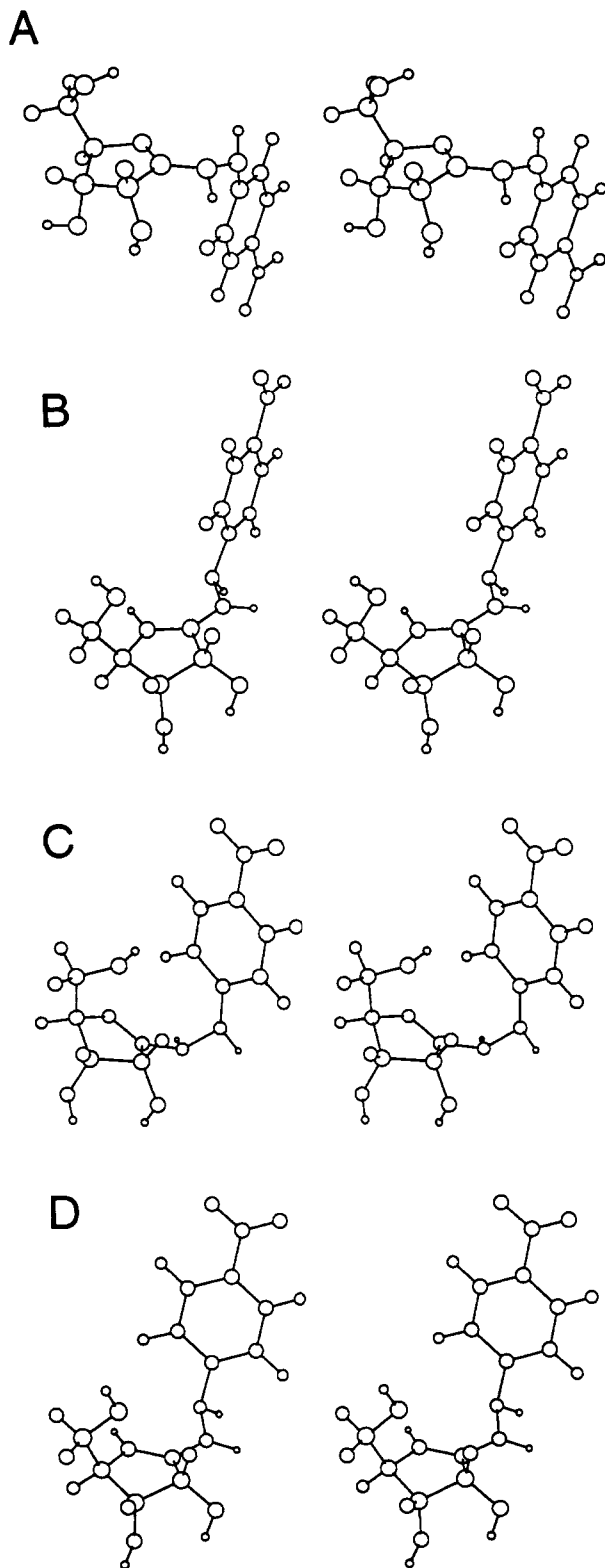
A

B

C

D

FIGURE 5: Stereoviews of (p-nitrophenyl)riboamidrazone 4 at global and local energy minima. The global energetic conformational minima for N$_4$'-unprotonated 4 is characterized by dihedral bond angles α = 299° and β = 338° (A). Protonation of N$_4$' results in a different energetic minimum, with α = 124° and β = 7° (B). A local energetic minimum for unprotonated 4, which places the conformation near that of the transition state, has α = 326° and β = 97° (C). Protonation at N$_4$' of 4 also permits the compound to reach a conformation near that of the transition state at a local energy minimum with α = 102° and β = 5° (D).

of the p-nitrophenyl plane relative to the plane of hypoxanthine at the transition-state. The conformation of 4 shown in Figure

5C places the p-nitrophenyl group in approximately the same plane as the departing hypoxanthine, while that in Figure 5D has the planes displaced by 2.5 Å. The conformers in Figure 5C,D represent structures 13.6 and 7.4 kcal, respectively, away from the global energetic minima shown in Figure 5A,B.

Due to uncertainties regarding the differential solvation between solution and enzyme-bound structures, these gas-phase calculations provide only qualitative values for conformational energetics. However, the structures are useful to provide guidance for inhibitor design where the aglycon is more favorably positioned for transition-state interactions.

DISCUSSION

Inhibition Constants for Amidrazones. The equilibrium dissociation constant K_i^* for (p-nitrophenyl)riboamidrazone 4 is 15-fold lower than that previously reported (Horenstein & Schramm, 1993b) for 1-(phenylimino)ribitol (2 vs 30 nM). Both compounds are slow-onset inhibitors. Phenylriboamidrazone 3 is bound with approximately the same affinity as 1-(phenylimino)ribitol (207 vs 170 nM). This latter pair both features oxocarbenium ion mimicry and contains the same phenyl group as a hydrophobic aglycon mimic. For nucleoside hydrolase, unlike some pyranoside exoglycosidases (Sinnott, 1990), the feature of planarity conferred by the amidrazone does not appear to be a major contributor to transition-state mimicry. However, the superior inhibition observed with (p-nitrophenyl)riboamidrazone 4 may be attributed to favorable H-bond-accepting interaction(s) not present in 1-(phenylimino)ribitol. An important feature of the transition-state for nucleoside hydrolase is protonation of the departing hypoxanthine ring at N7 (Horenstein et al., 1991, 1993a). The nitro group of the amidrazone inhibitor may be interacting with the enzymic proton donor, either by protonation or more likely by hydrogen bonding.

The energetics of binding of the (p-nitrophenyl)riboamidrazone have been investigated to estimate the energy change for folding the p-nitrophenyl group into the position occupied by the aglycon in the transition-state (compare B with C and D in Figure 1). Energy minimization studies indicate that the most favorable conformation for 4 results from extending the p-nitrophenyl group to the side of the heterocyclic ring. Rotation around the C–N and N–N bonds of the amidrazone to the position of the transition-state requires 7–14 kcal/mol for protonated or unprotonated 4.

Comparison of the Transition State for Nucleoside Hydrolase with (p-Nitrophenyl)riboamidrazone 4. Transition-state theory indicates that an inhibitor that is a perfect match for the transition-state structure will exceed the affinity of the Michaelis complex by a factor equivalent to the rate enhancement imposed by the enzyme, assuming that the enzymic rate enhancement is due to transition-state stabilization (Wolfenden, 1972). For N-glycohydrolases, the rate enhancement is approximately 6×10^{12} (DeWolf et al., 1979). The ideal transition-state inhibitor for nucleoside hydrolase would be expected to bind with an affinity of 6×10^{-17} M (Horenstein & Schramm, 1993b). Since the observed dissociation constant is 2×10^{-9} M for 4, and since the inhibitor must be distorted by 7–14 kcal/mol to bind in the transition-state conformation, an inhibitor of structure similar to 4 but with a conformational energy minimum near that shown in Figure 5 (lower stereo pairs) would be expected to bind with a dissociation constant in the range 10^{-14}–10^{-19} M. This value is in good agreement with the theoretical value for ideal transition-state binding. The total binding energy of the

transition-state interaction for nucleoside hydrolase is sufficiently large that even a conformationally unfavored analogue can be distorted by the transition-state binding energy and still provide extraordinary inhibition. Thus, the energy barrier of 7–14 kcal/mol to properly position the (*p*-nitrophenyl)-riboamidrazone at the catalytic site is easily provided by a fraction of the total potential binding energy of −17.8 kcal/mol for an ideal transition-state interaction.

An interesting feature of the conformational energy of (*p*-nitrophenyl)riboamidrazone is that different energetic barriers exist between the global minima for unprotonated and protonated **4** and the conformations that approximate the transition-state. At pH values within several units of the pK_a of 5.8, there are multiple routes by which to escape local energetic minima by protonation and deprotonation to permit the conformation to deform and, thus, to arrive at the conformation that mimics the transition state. Inhibition studies as a function of pH will be a useful method to identify the relative inhibitory power of protonated and unprotonated inhibitor. It is conceivable that flexible inhibitors like **4** may exhibit slow-onset inhibition by a time-dependent conformational change of the inhibitor instead of, or in addition to, an enzyme conformational change represented by k_5.

CONCLUSIONS

Recent advances in the ability to measure and interpret kinetic isotope effects for enzyme-catalyzed reactions provides geometric (Horenstein et al., 1991) and charge (Horenstein & Schramm, 1993a) information for enzymatic transition states. This information permits the comparison of inhibitor and transition-state features. An advantage of this approach is that protein structural information is unnecessary for logical inhibitor design. The potential for this approach is demonstrated with nucleoside hydrolase, where separate chemical designs have provided inhibitors of 2–30 nM (Horenstein & Schramm, 1993b; this work).

REFERENCES

Cleland, W. W. (1977) *Adv. Enzymol. Relat. Areas Mol. Biol.* *45*, 273–387.

DeWolf, W. E., Jr., Fullin, F. A., & Schramm, V. L. (1979) *J. Biol. Chem.* *254*, 10868–10875.

Endo, Y., Gluck, A., & Wool, I. G. (1991) *J. Mol. Biol.* *221*, 193–207.

Ganem, B., & Papandreou, G. (1991) *J. Am. Chem. Soc.* *113*, 8984–8985.

Horenstein, B. A., & Schramm, V. L. (1993a) *Biochemistry 32*, 7089–7097.

Horenstein, B. A., & Schramm, V. L. (1993b) *Biochemistry 32*, 9917–9925.

Horenstein, B. A., Parkin, D. W., Estupinan, B., & Schramm, V. L. (1991) *Biochemistry 30*, 10788–10795.

Ikota, N., & Hanaki, A. (1990) *Chem. Pharm. Bull. 38*, 2712–2718.

Leung, H. B., & Schramm, V. L. (1980) *J. Biol. Chem. 255*, 10867–10874.

Mentch, F., Parkin, D. W., & Schramm, V. L. (1987) *Biochemistry 26*, 921–930.

Merkler, D. J., Brenowitz, M., & Schramm, V. L. (1990) *Biochemistry 29*, 8358–8364.

Morrison, J. F., & Stone, S. R. (1985) *Comments Mol. Cell. Biophys. 2*, 347–368.

Morrison, J. F., & Walsh, C. T. (1988) *Adv. Enzymol. Relat. Areas Mol. Biol. 61*, 201–301.

Munns, A. R. I., & Tollin, P. (1970) *Acta Crystallogr. B26*, 1101–1113.

Papandreou, G., Tong, M. K., & Ganem, B. (1993) *J. Am. Chem. Soc. 115*, 11682–11690.

Parkin, D. W., Horenstein, B. A., Abdulah, D. R., Estupinan, B., & Schramm, V. L. (1991) *J. Biol. Chem. 266*, 20658–20665.

Sancar, A., & Sancar, G. B. (1988) *Annu. Rev. Biochem. 57*, 29–67.

Sinnott, M. L. (1990) *Chem. Rev. 90*, 1171–1202.

Tarmus, C., Muller, H. M., & Schuber, F. (1988) *Bioorg. Chem. 16*, 38–51.

Tong, M. K., Papandreou, G., & Ganem, B. (1990) *J. Am. Chem. Soc. 112*, 6137–6138.

Wolfenden, R. (1972) *Acc. Chem. Res. 5*, 10–18.